Generating MnO₂ Nanoparticles Using Simulated Amorphization and Recrystallization

Thi X. T. Sayle,[†] C. Richard A. Catlow,[‡,§] R. Regina Maphanga,[†,||]
Phuti E. Ngoepe,[||,⊥] and Dean C. Sayle*,[†]

*Contribution from the DEOS, Cranfield University, Defense Academy of the U.K., Shrivenham,
Swindon, U.K., The Royal Institution of Great Britain, 21 Albemarle Street, London, U.K.,
Department of Chemistry, University College London, U.K., Materials Modeling Center,
School of Physical and Mineral Sciences, University of Limpopo, P/Bag X 1106,
Sovenga 0727, South Africa, and Manufacturing and Materials Technology,
Council for the Scientific and Industrial Research, P.O. Box 392, Pretoria 0002, South Africa*

Received November 1, 2004; E-mail: d.c.sayle@cranfield.ac.uk

Abstract: Models of MnO₂ nanoparticles, with full atomistic detail, have been generated using a simulated amorphization and recrystallization strategy. In particular, a 25,000-atom "cube" of MnO₂ was amorphized (tension-induced) under molecular dynamics (MD). Long-duration MD, applied to this system, results in the sudden evolution of a small crystalline region of pyrolusite-structured MnO₂, which acts as a nucleating "seed" and facilitates the recrystallization of all the surrounding (amorphous) MnO₂. The resulting MnO₂ nanoparticle is about 8 nm in diameter, conforms to the pyrolusite structure (isostructural with rutile TiO₂, comprising 1 × 1 octahedra) is heavily twinned and comprises a wealth of isolated and clustered point defects such as cation vacancies. In addition, we suggest the presence of ramsdellite (2 × 1 octahedra) intergrowths. Molecular graphical snapshots of the crystallization process are presented.

Introduction

There is growing interest in the study of manganese oxides as a result of, among other factors, their importance as components of solid-state battery systems. An important class is the dioxides, MnO₂, of which there are over 14 polymorphs.[1] These are useful materials because they comprise internal tunnel structures with sizes commensurate with that of cations spanning "proton" to cesium[2] and can therefore act as host lattices for the insertion and extraction of cations, and hence charge,[3] which is central to their electrochemical performance.[4]

Perhaps the best-known polymorph is electrochemically active γ-MnO₂, which is widely used as the cathode material in primary alkaline batteries.[1] γ-MnO₂ comprises a complex *microstructure*, which includes (i) de Wolff disorder (intergrowths of pyrolusite and ramsdellite[1]), (ii) microtwinning,[5] and (iii) point defects[6] such as Mn⁴⁺ vacancies and Mn³⁺ substitutionals. Consequently, this microstructure results in complex and variable X-ray diffraction patterns (XRD),[6] and full characterization at the

atomistic level is difficult experimentally. At present, there is no efficient method of characterizing industrial samples of γ-MnO₂ and, thereby, no means of relating their atomistic scale arrangement with their behavior in batteries. For example, the pyrolusite/ramsdellite intergrowths are likely to influence the properties of the material such as electrical conductivity,[7] ion-exchange,[8] ion-absorption,[9] and gas reactivity[10] all of which are central to its utilization within battery systems. In this study, we use simulation and modeling techniques to help experiment understand and characterize the microstructural complexities of γ-MnO₂.

Many theoretical studies used to investigate the structure and energetics of a system proceed by proposing an atomistic model, which is then simulated using static or dynamical methods. However, for systems that comprise complex microstructures, such as γ-MnO₂, the starting structural models can be difficult to generate. For example, the model needs to include within a *single* simulation cell: (i) ramsdellite/pyrolusite intergrowths, the interfacial configuration of these intergrowths and the relative sizes of the domains—this is certainly a challenging undertaking in itself. One then needs to ensure that "some" of the domains are (ii) twinned, and finally (iii) point defects need to be introduced. Moreover, all microstructural features (i), (ii), and (iii) are associated with combinations and permutations associated with location, arrangement, and concentration. Not-

[†] Cranfield University.
[‡] The Royal Institution of Great Britain.
[§] University College London.
[||] University of Limpopo.
[⊥] Council for the Scientific and Industrial Research.

(1) Chabre, Y.; Pannetier, J. *Prog. Solid State Chem.* **1995**, *23*, 1.
(2) Tang, W.; Yang, X.; Liu Z.; Ooi, K. *J. Mater. Chem.* **2003**, *13*, 2989.
(3) Manickam, M.; Singh, P.; Issa, T. B.; Thurgate, S.; De Marco, R. *J. Power Sources* **2004**, *130*, 254.
(4) Whittingham, M. S.; Zavalij P. Y. *Solid State Ionics* **2000**, *131*, 109.
(5) MacLean, L. A. H.; Tye, F. L. *J. Solid State Chem.* **1996**, *123*, 150.
(6) Hill, J.-R.; Freeman, C. M.; Rossouw, M. H. *J. Solid State Chem.* **2004**, *177*, 165.

(7) Li, J. B.; Koumoto, K.; Yanagida, H. *J. Ceram. Soc. Jpn.* **1988**, *96*, 74.
(8) Wadsley A. D. *J. Am. Chem. Soc.* **1950**, *72*, 1981.
(9) BigLiocca, C.; Giraidi, F.; Pauly, J.; Sabioni, E. *Anal. Chem.* **1967**, *39*, 1634.
(10) Li, J. B.; Koumoto, K.; Yanagida, H. *J. Mater. Sci. Lett.* **1988**, 331.

Table 1. Potential Parameters Describing the Short-Range Potential Terms between the Component Ion Species of $MnO_2{}^a$

interaction	A (Å)	ρ (Å)	C (eVÅ⁻⁶)	species	q(e)
$Mn^{2.2+}-Mn^{2.2+}$	23530.50	0.156	16.00	$Mn^{2.2+}$	2.20
$Mn^{2.2+}-O^{1.1-}$	15538.20	0.195	22.00		
$O^{1.1-}-O^{1.1-}$	11782.76	0.234	30.22	$O^{1.1-}$	−1.10

[a] q is the partial charge on the ion; a short-range cutoff of 10.0 Å was used. These potentials reproduce the lattice parameters' of pyrolusite and ramsdellite to within, respectively, 3% and 4% of experiment (see Supporting Information) and predict that the pyrolusite polymorph is more stable.[21]
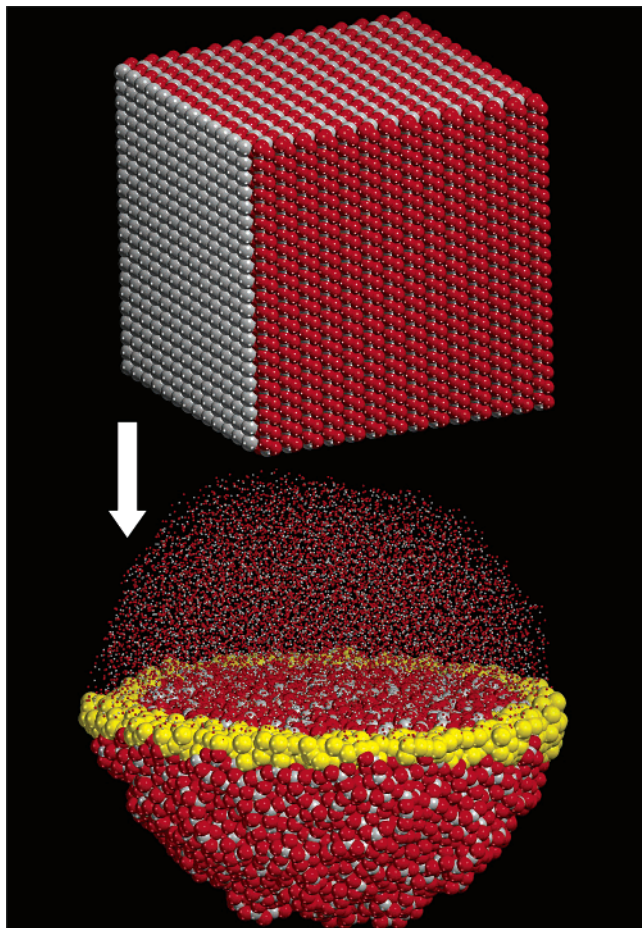

Figure 1. Graphical representation of the atom positions comprising: (top) starting configuration; (bottom) amorphous configuration, calculated after 500 ps. Oxygen (red); manganese (gray). To show more clearly the amorphous configuration, the ions comprising the top half the nanoparticle are shown with smaller diameter spheres. In addition, the pseudospherical shape of nanoparticle is made clearer by coloring some of the ions yellow.

withstanding this daunting task, Hill, Freeman, and Rossouw[6] attempted just this. In particular, these authors generated hundreds of systems comprising random arrays of ramsdellite and pyrolusite, which were then simulated by energy minimization using ion-pair potential models. The XRD pattern for each system was then calculated and compared with experimental XRD patterns to establish whether the model generated was structurally realistic. The authors concluded that the major microstructural feature of γ-MnO₂ is de Wolff disorder. This study is a very elegant example of how experimental data, coupled with atomistic computer simulations, can elucidate detailed atomistic configurations, which neither simulation nor experiment could ascertain individually.
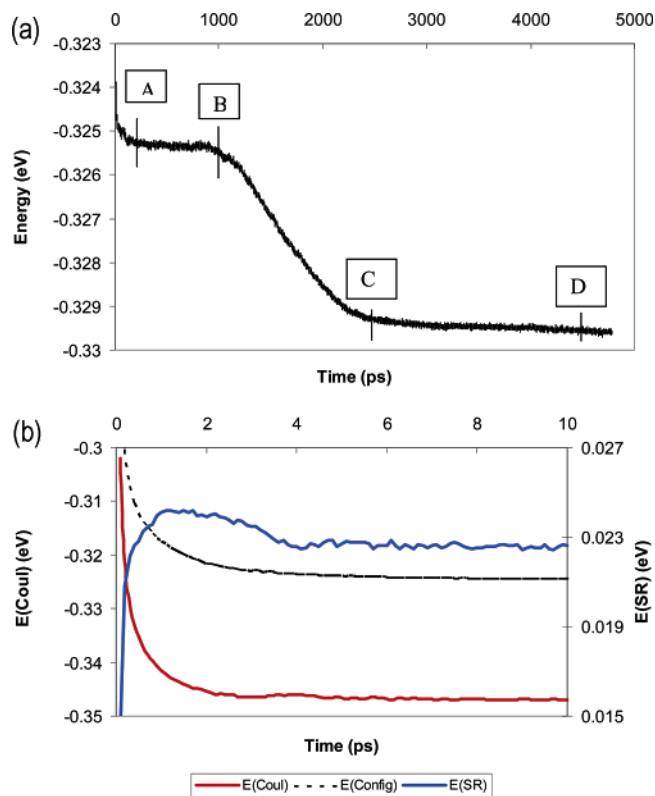

Figure 2. Calculated energy ($\times 10^6$) of the nanoparticle (at 2000 K). (a) Configurational energy, E(Config); (b) Coulombic, E(Coul) left ordinate, and short range, E(SR) right ordinate, components to the configurational energy, E(Config) left ordinate, calculated as a function of time. (b) Same as (a) but follows only the first 10 ps in time. We do not know if there is any significance in the plateau time (a) Points A, B. We *suggest* that it may be the (random) time taken to evolve a "seed" to facilitate crystallization. At point C, the nanoparticle is fully crystalline. However, inspection of the trace, point C−D, reveals that the configurational energy is still reducing. Accordingly, this part of the simulation, C−D, may be regarded as simulated annealing.

A different approach, and one that we consider in this present study, is to use evolutionary simulation. Here, it is the simulation itself that directs the atomistic configuration, where the simulation is based upon some evolutionary procedure, which may include, for example, nucleation and growth or genetic algorithms based upon rules such as: "survival of the fittest".[11−15] These evolutionary approaches negate, in part, the need to construct an initial model, which helps eliminate the possibility of generating incorrect structures by making, perhaps erroneous, assumptions pertaining to the structure based upon, for example, chemical intuition. In this study, we use an evolutionary method: "amorphization and recrystallization"[11] to generate models of MnO₂, which comprise complex microstructures. This is a first step in helping experiment characterize γ-MnO₂ with an aim, ultimately, of being able to correlate (micro)structure with properties. In addition, we explore the structure of nanoparticles of MnO₂. Indeed, there is growing interest in the study of MnO₂ nanomaterials;[16−19] the promise of unique

(11) Sayle, D. C.; Johnston, R. L. *Curr. Opin. Solid State Mater. Sci.* **2003**, *7*, 3.
(12) Pannetier, J.; Bassas-Alsina, J.; Rodriguez-Carvajal, J.; Caignaert, V. *Nature* **1990**, *346*, 343.
(13) Bush, T. S.; Catlow C. R. A.; Battle, P. D. *J. Mater. Chem.* **1995**, *5*, 1269.
(14) Woodley, S. M.; Battle, P. D.; Gale, J. D.; Catlow, C. R. A. *Phys. Chem. Chem. Phys.* **2004**, *6*, 1815.
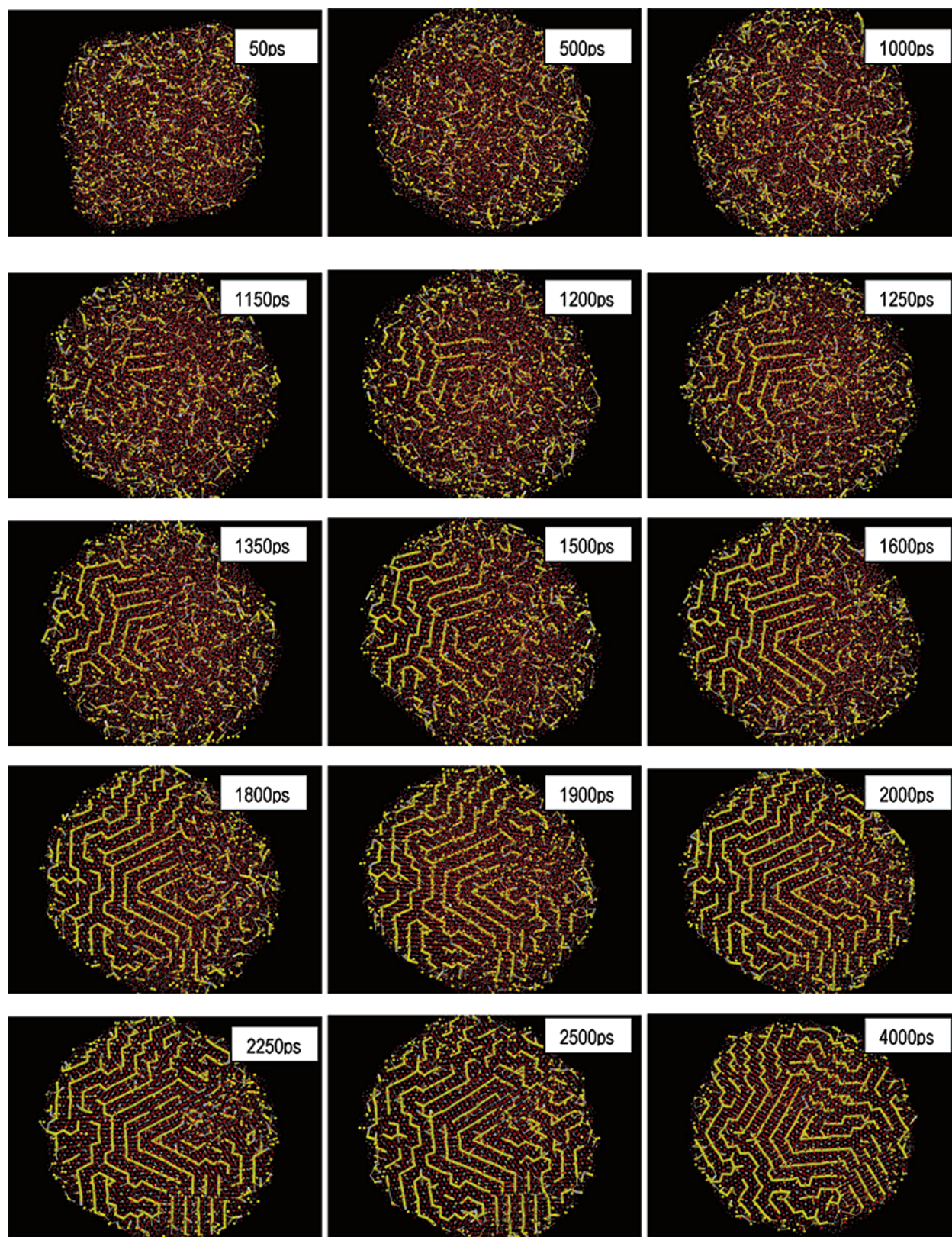(15) Woodley, S. M.; Catlow, C. R. A.; Battle, P. D.; Gale, J. D. *Chem. Commun.* **2004**, 22. [

Figure 3. Snaphots of the atom positions comprising the MnO_2 nanoparticle, taken as a function of time, illustrating the crystallization process. Species colored yellow correspond to manganese and are bonded to each other to illustrate more clearly the crystallinity, connectivity, and evolution of twinning. The figures were constructed to ensure clarity of the crystallization process and therefore most of the ions comprising the nanoparticle are shown as dots. The time, shown in ps, is usefully correlated with the energy trace in Figure 2. Manganese ions are colored yellow, oxygen ions are red.

structural and property changes as one traverses down to the nanoscale (and hence possible exploitation and associated applications) is certainly an enticing and exciting prospect.

Theoretical Methods

In this section, we describe briefly, the potential models used to describe the interactions between the Mn and O ions comprising MnO₂, the simulation code used to perform the dynamical simulation, and finally, the construction of the nanoparticle and its amorphization and subsequent recrystallization.

Potential Models. All calculations presented in this study are based on the Born model of the ionic solid, in which the Mn and O ions interact via long-range Coulombic interactions and short-range parametrized interactions. We employ a rigid ion model, with partial charges. The potentials were obtained by modifying the parameters developed by Matsui[20] for isostrutural rutile-TiO₂ so that they gave good agreement with the crystal structures of both pyrolusite and ramsdellite;[21] the pyrolusite polymorph is calculated to be more stable than ramsdellite. The analytical form of the force field is simple and readily suited to numerically demanding dynamical simulations. The analytical expression, describing the interaction, U, between two ions, i and j, of charge q and separated by a distance, r, is given in eq 1 below:

$$U_{r_{ij}} = \left[\frac{q_i q_j}{r_{ij}} + A_{ij} \, e^{(-r_{ij}/\rho_{ij})} - \frac{C_{ij}}{r_{ij}^6} \right] \qquad (1)$$

The potential parameters are presented in Table 1.

Simulation Code. The DL_POLY code[22] was used in this study to perform all the dynamical simulations. This code utilizes three-dimensional periodic boundary conditions, and therefore the nanoparticle was placed in the center of a 3D periodic box, which was sufficiently large to ensure that the interactions between its neighboring images are negligible. All simulations were performed within the NVE ensemble. Instantaneous velocity scaling to the simulation temperature was used throughout. This procedure prevents the rapid and large buildup of excess kinetic energy as the nanoparticle evolves from the highly strained (tensioned) initial configuration, via the amorphous transition, to a crystalline phase with reduced strain and a range of defects.

Amorphization and Recrystallization Strategy. If one simulates MnO₂ by applying molecular dynamics (MD) simulation to the *crystalline* material, the Mn and O ions will simply vibrate about their lattice sites. This is because the barrier heights in ceramics are typically of the order of 1 eV. Thus, the time required to run the simulation to observe (statistically) an *event* (i.e. an ion moving off its lattice position to occupy a different position), at 1000 K, is about 0.1 μs. Typically, this is a far longer time scale than can be accommodated, with available computational facilities, using MD. Conversely, in a molten system, the ions are highly mobile because the barrier heights are much lower. In the amorphization and recrystallization strategy, we exploit this high ionic mobility. In particular, an amorphous configuration is generated in which the ions have high mobility, similar to those within a molten system. The system is then allowed to recrystallize, during which time
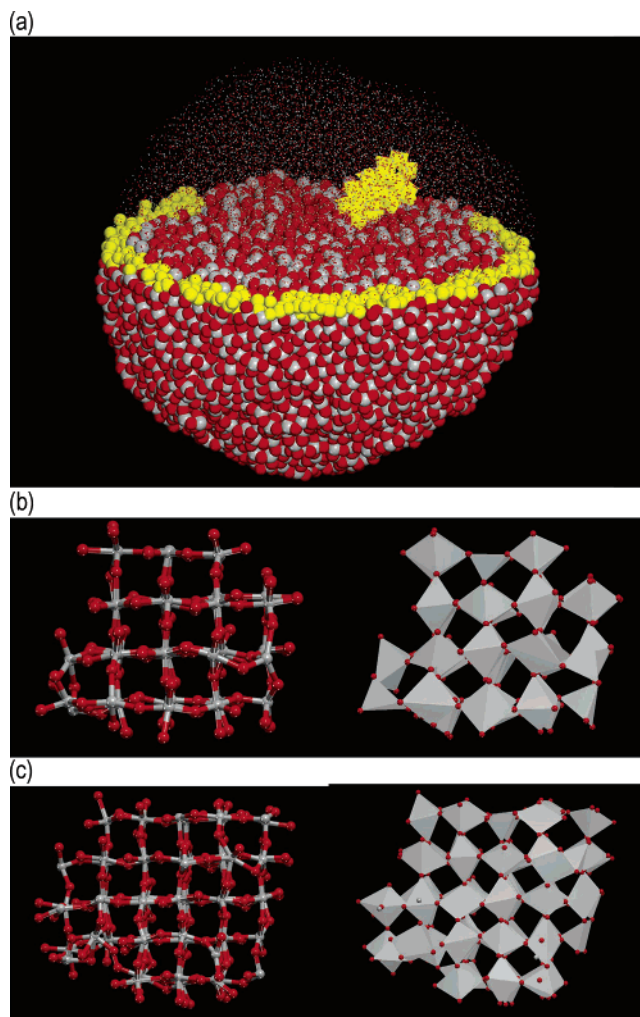
(16) Malik, A.-S.; Duncan, M. J.; Bruce, P. G. *J. Mater. Chem.* **2003**, *13*, 2123.
(17) Yuan, Z.-Y.; Zhang, Z.; Du, G.; Ren T.-Z.; Su. B.-L. *Chem. Phys. Lett.* **2003**, 378.
(18) Wu, C.; Xie, Y.; Wang, D.; Yang J.; Li, T. *J. Phys. Chem. B* **2003**, *107*, 13583.
(19) Kobayashi, S.; Kottegoda, I. R. M.; Uchimoto, Y.; Wakihara, M. *J. Mater. Chem.* **2004**, *14*, 1843.
(20) Matsui M.; Akoagi M. *Mol. Simul.* **1991**, *6*, 239.
(21) Maphanga, R. R. Ph.D. Thesis, 2005, University of the North, Sovenga 0727, South Africa.
(22) Smith, W.; Forester, T. R. *DL_POLY*; a package of Molecular Simulation routines; Council for the Central Laboratory of the Research Councils, Daresbury Laboratory: Daresbury, Warrington, UK, 1996; http://www.dl.ac.uk/TCSC/Software/DLPOLY.

Figure 4. Configuration of the crystalline MnO₂ "seed", that evolved within the amorphous nanoparticle: (a) location of the MnO₂ "seed" (yellow); (b) atomistic structure of the seed after 750 ps; (c) after 850 ps. To the left of (b) and (c) a ball-and-stick representation of the ion positions is shown; to the right, the corresponding Mn octahedra are depicted, illustrating more clearly the pyrolusite structure of the MnO₂. Color notation as Figure 1.

the ions have sufficiently high mobilities to allow them to move into low-energy configurations within the time scales (typically nanoseconds) accessible to the simulation. The material, as it recrystallizes, will evolve microstructural features observed experimentally, including for example, grain-boundaries, dislocations, point defects, surface structures, faceting, and morphology.[23−25] Amorphization and recrystallization is therefore an appropriate simulation tool with which to explore systems with complex microstructures, such as γ-MnO₂, because it does not require one to propose and generate an atomistic structure that includes all the microstructural features, prior to simulating with dynamical or static methods.

The amorphous transition can be induced via tension or compression. For example, a 10% compression-induced amorphization would involve changing the coordinates of all the ions comprising the system to facilitate a 10% reduction in the lattice parameter. Clearly, this is a high-energy configuration because of the repulsive interactions between the component ions. Consequently, when MD is applied, the ions repel each other and move (accelerate) in an attempt to restore the normal bond distances/lattice parameter. This can have various consequences:

(23) Sayle, D. C. *J. Mater. Chem.* **1999**, *9*, 2961.
(24) Sayle, D. C.; Watson, G. W. *Surf. Sci.* **2001**, *473*, 97.
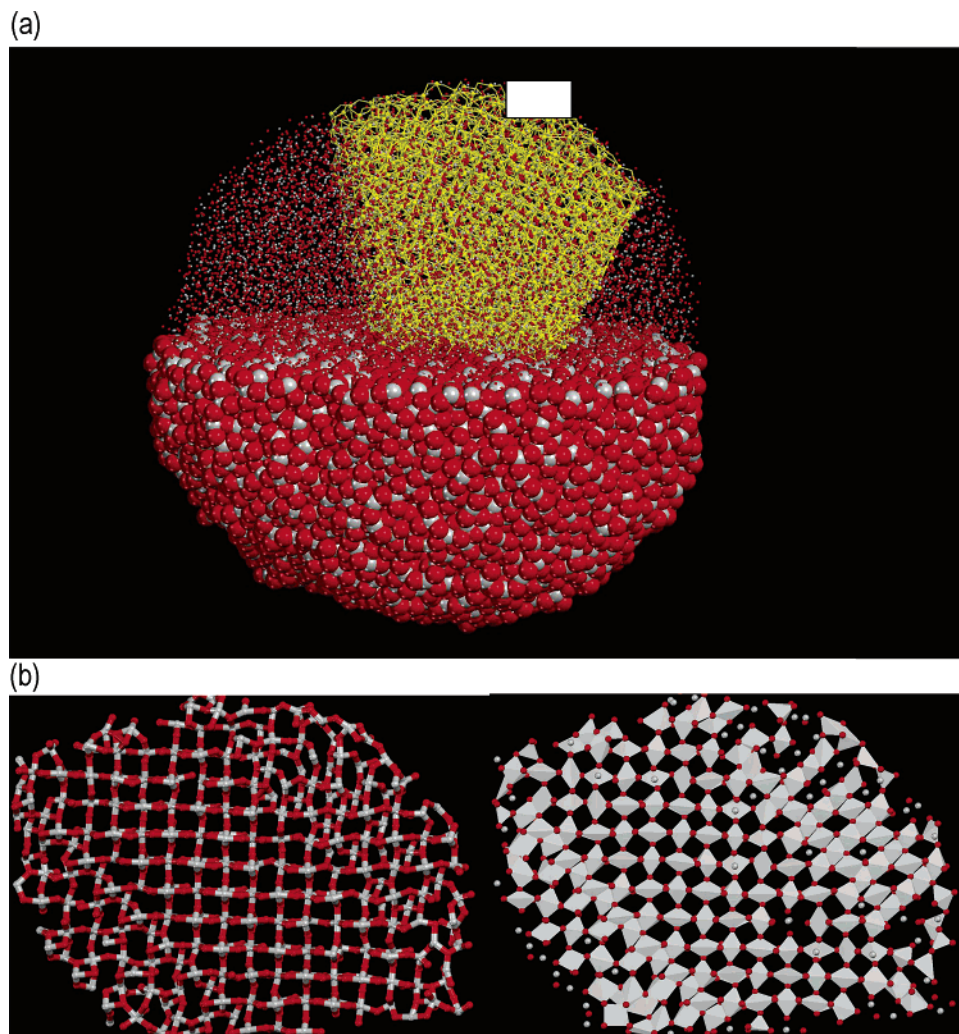(25) Sayle, T. X. T.; Parker S. C.; Sayle, D. C. *Chem. Commun.* **2004**, 2438.

Figure 5. Representations of the atom positions illustrating the initial stages of twinning within the crystalline MnO_2 and taken after 1750 ps of dynamical simulation: (a) location of the crystalline region (yellow), with respect to the rest of the nanoparticle, usefully compared with Figure 4a−c; (b) ball-and-stick (left) and polyhedral (right) representation. Color rendition as in Figure 1.

(i) The ions all move back immediately to restore the equilibrium bond distances and lattice parameter. This simply reverts the structure back to the starting position. Clearly, no useful information is derived here.

(ii) The compression is sufficient to cause a "partial amorphization". Here, some of the ions move off their lattice positions under MD and the system may appear amorphous. However, particular domains of the material remain crystalline throughout the simulation. Typically, one might observe, for example, lattice slip within the structure, the evolution of point defects and the formation of steps/ledges at the surface, which change the crystal morphology.[21]

(iii) The accelerations of the ions and subsequent collisions between the ions comprising the nanoparticle are sufficient to ensure that *all* the ions move off their lattice position. This effectively removes all long-range order from the system and this we term a "full amorphization".

(iv) The initial compression is so high that the ions accelerate and collide with such magnitude that the simulation fails catastrophically.

Clearly, only (ii) and (iii) deliver useful results; in this study we induce a full amorphization. During the amorphization stage, velocity scaling, to the simulation temperature, is used throughout to remove the excess energy associated with the initial compression and to prevent the system from vaporizing.

The compression required to achieve a successful amorphization is sensitive to the system of study (i.e. MnO_2) and potential model used to describe it, and to the temperature at which the simulation is run. For some systems, for example amorphization of CeO_2 nanoparticles,[25] we could find no compressions that amorphized effectively the nanoparticle; rather, successful amorphization was only achieved if tension induced.

Once the amorphous structure has been generated, one needs then to recrystallize the system. This is influenced primarily by the temperature at which the MD is run: If the temperature is too high, the system melts. Conversely, the system will not recrystallize (within time scales accessible using available computational facilities) if the temperature is too low. The conditions required achieving a successful (full) amorphization and subsequent recrystallization are given in the following section.

Nanoparticle Generation. A "cube" of pyrolusite, comprising 24,696 atoms, was constructed. The coordinates of all the ions comprising this cube were then changed to *increase* (tension-induced amorphization) the lattice parameter by 36%. Dynamical simulation (MD), with a time step of 0.005 ps, was then performed on this system at 2000 K for 4000 ps during which times the nanoparticle amorphized and subsequently recrystallized. Finally, the system was cooled gradually: MD was run for 500 ps at 1500 K, 250 ps at 1000 K, 250 ps at 500 K and 500 ps at 0 K, the latter acts effectively as an energy minimization. This simulation required about 5 days using 96 processors of a SunFire F15K Galaxy-class configuration supercomputer.
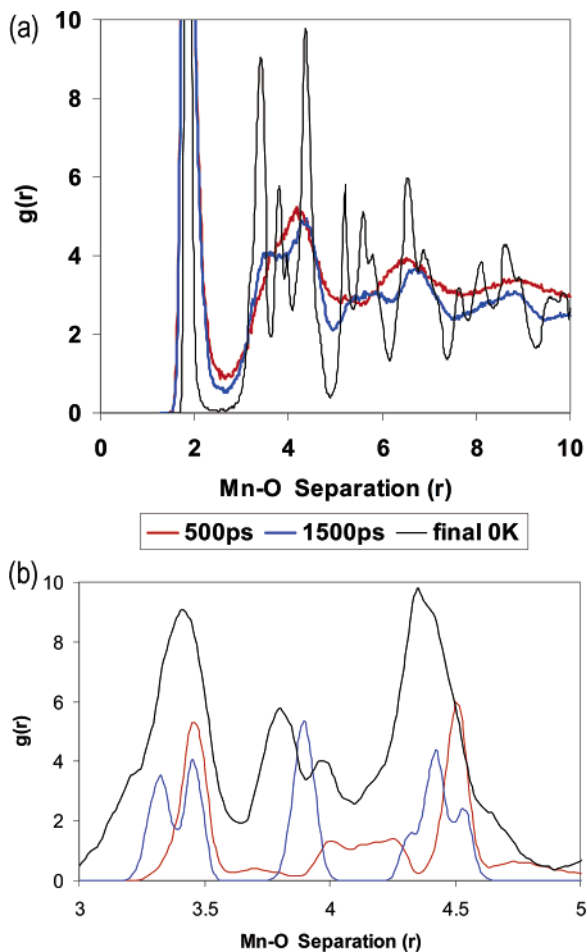
Figure 6. (a) Mn−O RDF calculated after 500 ps (amorphous structure), 1500 ps (partially recrystallized) and at the end of the simulation; (b) Mn−O RDF calculated at the end of the simulation (black trace) compared with the parent pyrolusite (blue trace) and ramsdellite (red) materials; the RDF for the parent materials are not from crystallographic data taken from experiment, rather they were calculated based upon the (potential) models used to describe the pyrolusite and ramsdellite polymorphs. Note the Mn−O separation for (b) runs from 3 to 5 Å rather than 0−10 Å for (a).
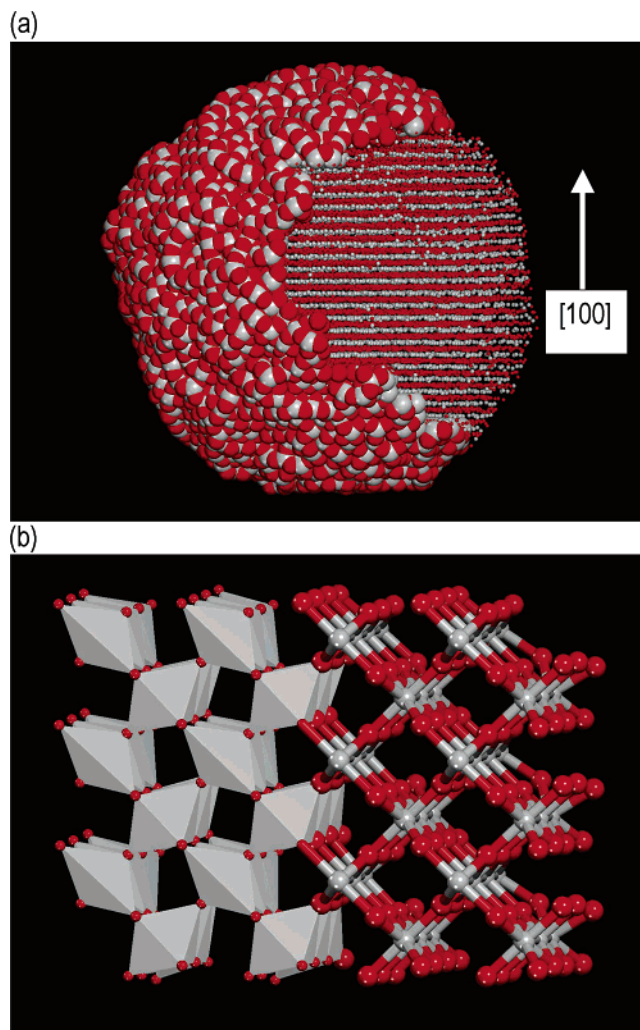
Figure 7. Graphical representation of the atom positions comprising the final, 0 K, structure of the nanoparticle: (a) sphere model representation, some of the spheres are reduced in size to show the stacking of the Mn and O planes along the [100]; (b) segment of the nanoparticle, cut from (a) illustrating more clearly the pyrolusite structure. (Left) Polyhedral rendering of the Mn ions. (Right): Ball-and-stick representation. Manganese (gray); oxygen (red).

Results

The starting crystalline structure and amorphous configuration of the MnO₂ is shown in Figure 1; the corresponding configurational energy of the system, calculated during MD performed at 2000 K, is presented in Figure 2.

Immediately after MD is applied to the highly tensioned nanoparticle, the component ions move with considerable acceleration to reduce the lattice parameter (the system can perhaps be likened to an elastic band under tension, which is then released). We note that no constraints on the ions are imposed after the MD has started; rather, it is only the starting configuration that is tensioned. The short-range (repulsive), $E(SR)$, and Coulombic, $E(Coul)$, components of the configurational energy, $E(Config)$, are shown in Figure 2b for the first 10 ps of MD. As the ions accelerate back, $E(SR)$, increases, as one might expect. However, this is countered by a decrease in $E(Coul)$. In total, $E(Config)$ becomes more negative (more stable) because the Coulombic terms far outweigh $E(SR)$, as one can observe from Figure 2b. After about 200 ps, $E(Config)$ plateaus, Figure 2a, point A. Inspection of the ion positions after 500 ps, Figure 1, reveals an amorphous "spherical" nanoparticle.

Clearly, the energy *associated* with tensioning the system by 36% was sufficient to amorphize the nanoparticle.

The plateau in the configurational energy, Figure 2, continues until about 1000 ps, point B, at which point $E(Config)$ starts to become more negative again. Close inspection of the ions comprising the nanoparticle reveals that this sudden reduction in the energy corresponds to the start of the recrystallization of the nanoparticle. This crystallization continues until point C where the energy plateaus again. The crystallization process therefore takes about 1500 ps to complete.

A movie of the atom trajectories was generated, using molecular graphical techniques. The animation revealed, with 3D atomistic detail, the crystallization process (from point A to point C in Figure 2a). In Figure 3, snapshots of the movie are depicted after various times to help describe the crystallization process. Moreover, because each frame of the movie contains the coordinates and trajectory details of 24,696 atoms, molecular graphics visualization was central to this study.

The velocities of the ions were scaled to the simulation temperature throughout the simulation. This procedure draws
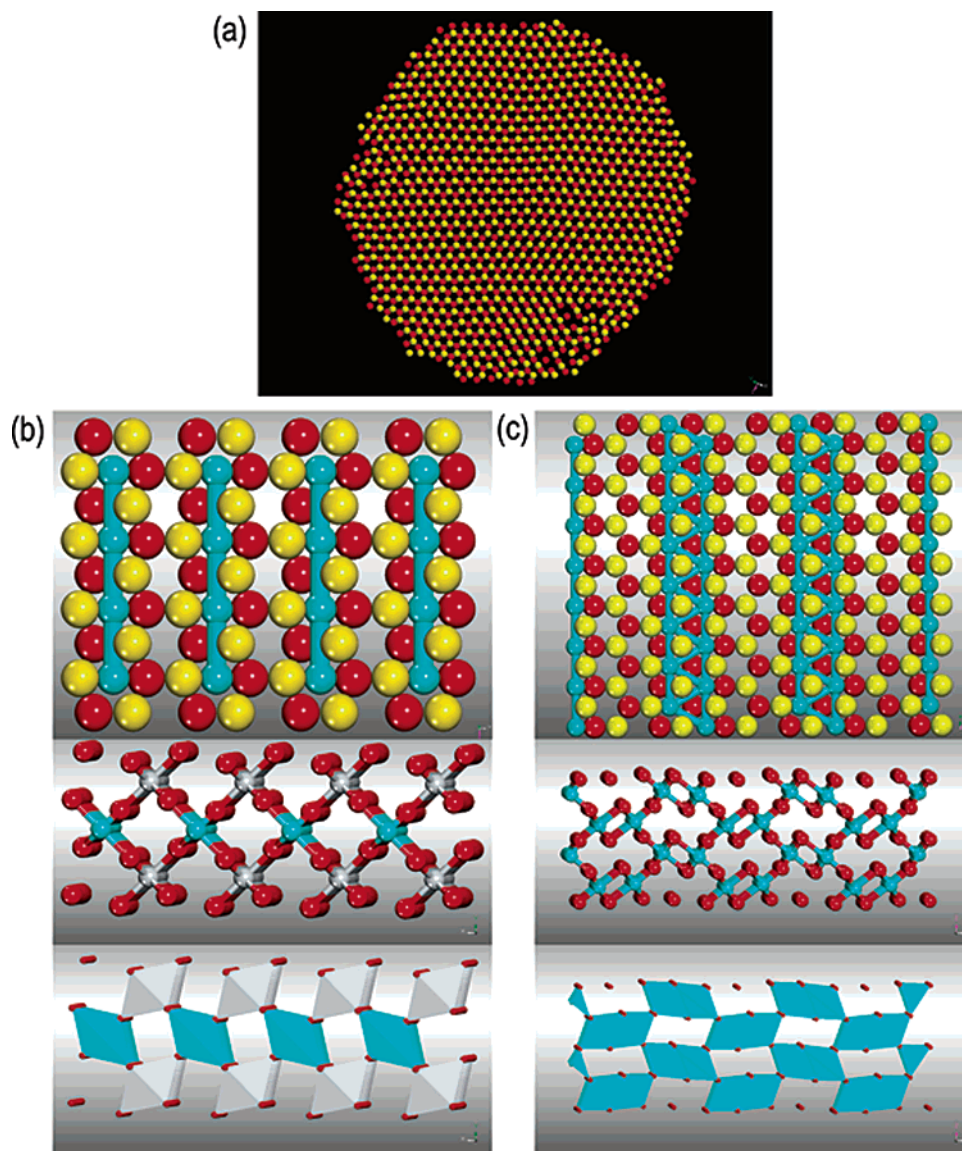
Figure 8. (a) Sphere model representation of a slice, cut through the nanoparticle perpendicular to [100], showing two oxygen layers and the octahedral sites they give rise to (the Mn have been removed to aid clarity). Yellow spheres represent oxygen ions lying "above" the plane of the paper; red spheres are those lying "below" the plane of the paper; (b) schematics describing the pyrolusite structure; (c) schematics describing the ramsdellite structure. Note (b) and (c) are from crystallographic data and NOT from our calculations. In (b) and (c), Mn are colored blue or gray to aid clarity.

the excess energy, arising from the latent heat of crystallization, away from the system and therefore helps prevent vaporization or re-amorphization. This process can be likened to heat exchange between "the system" and its environment in experiment.

The snapshots, Figure 3, show the simulated crystallization process. In particular, the figure suggests that the nanoparticle grows from a *single* initial crystalline "seed" that can be observed to have evolved at about 1150 ps. The structure of this seed was examined in closer detail and the movie extrapolated back (prior to 1150 ps) to identify visually, from our simulation, the smallest size of seed that was crystalline. The structure of this "nucleating seed", observed at 750 ps, is shown in Figure 4 and conforms to the pyrolusite structure (isostructural with rutile TiO_2). Prior to 750 ps, no crystalline "seed" could be identified. After 850 ps, the seed has clearly grown in size, Figure 4c, as ions within the surrounding (amorphous) region crystallize around it.

After 1750 ps, the crystalline region is much larger and is shown in Figure 5. It is apparent from inspection of this figure that microtwinning has occurred. In particular, close inspection of the snapshots (Figures 3−5) reveals that the Mn crystallizes into octahedral holes not only in a straight/parallel fashion, which propagates the pyrolusite structure, but also at specific angles, which results in the formation of the twin boundaries. Inspection also reveals that the crystallization proceeds from a *single* crystalline seed; it is conceivable that two or more seeds could have evolved with crystallization fronts emanating from both seeds.

In Figure 6, the Mn−O radial distribution function (RDF) of the nanoparticle after 500 ps (at 2000 K) and at the end of the simulation (0 K) is shown. The figure shows clearly the amorphous transition, characterized by broad peaks in the RDF. The final structure comprises sharp, well-resolved peaks characteristic of a crystalline material. The RDF after 1500 ps is also shown to illustrate the transition from the amorphous to
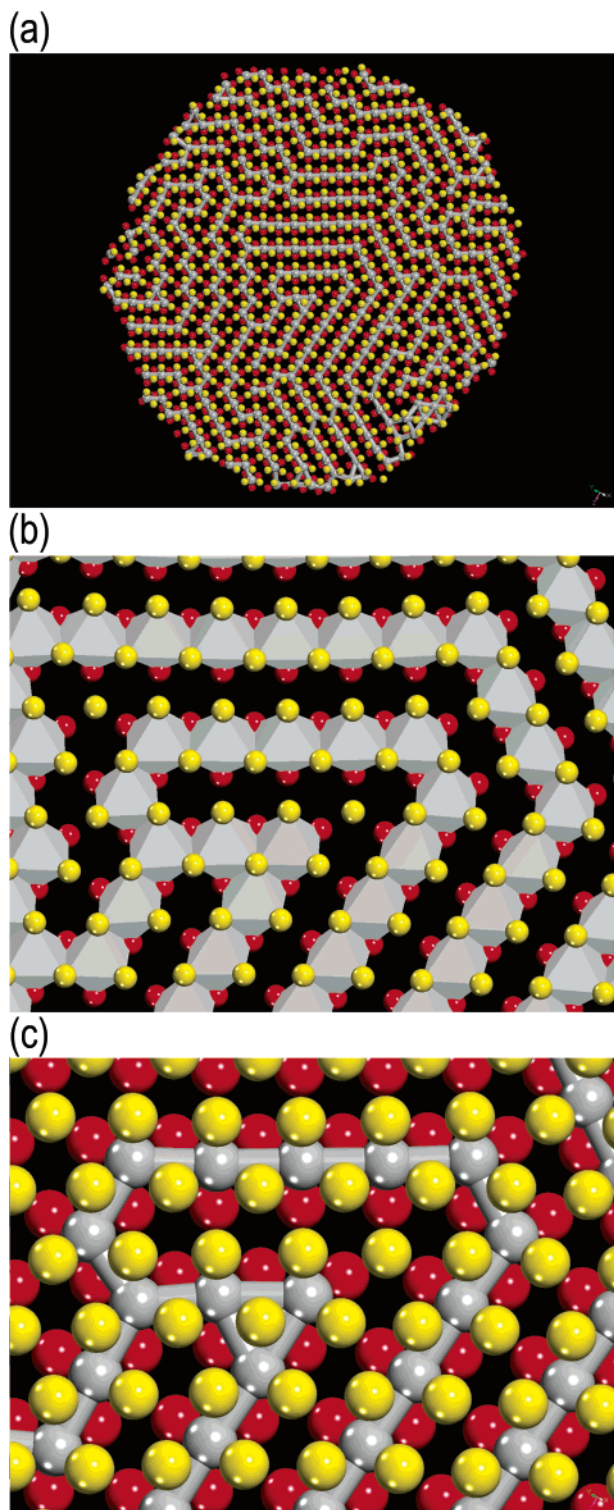
Figure 9. As in Figure 8a above, with the Mn ions included. (a) Sphere model representation of the whole slice; (b) enlarged segment of (a) with polyhedral rendering of the Mn ions; (c) enlarged segment of (b) with ball-and-stick rendering of the Mn ions.

the crystalline configuration. In particular, the (partially crystal-line) trace is similar to the 500 ps (amorphous) but with a few additionally resolved peaks. The 1500 ps trace remains broad owing to the contribution of the remaining amorphous regions to the RDF. In Figure 6b, the RDF, calculated for the final, 0 K, nanoparticle structure is compared with the RDF calculated for the (simulated) parent pyrolusite (blue) and ramsdellite (red)

materials. The correlation between the RDF does not favor either material; rather we suggest that the MnO₂ nanoparticle has structural characteristics of both the ramsdellite and pyrolusite structures. Inspection of the final, 0 K structure, shown in Figure 7, reveals a crystalline nanoparticle, which accommodates predominantly domains that confirm to the pyrolusite structure.

The structure of the nanoparticle is highly complex and is not a single crystal; rather, it comprises a wealth of twin boundaries. To understand more clearly the twinning within the nanoparticle, a slice was cut through the middle of the nanoparticle, Figure 7a, and perpendicular to [100]. The slice, which comprises two oxygen layers, is shown in Figure 8; the layer of Mn ions, which are sandwiched between the two oxygen layers have been removed for clarity. The figure is shown with the [100] perpendicular to the plane of the paper. The two oxygen layers give rise to octahedral sites, which lie at the center of each of the hexagons formed by the oxygen ions. The filling of these octahedral sites leads to either the pyrolusite structure, Figure 8b, and/or the ramsdellite structure, Figure 8c. We note that b and c of Figure 8 are for reference only and are taken from crystallographic data. They are NOT from the coordinates extracted from the nanoparticle simulation in this present study. In Figure 9a the two oxygen planes are again shown, as Figure 8a, but this figure includes also the Mn ions sandwiched between. Figure 9b shows an enlarged segment of 9a with the Mn depicted by use of polyhedral rendering; 9c is a slight enlargement of 9b with ball-and-stick rendering of the Mn layer. It is evident from inspection of Figure 9 that the pyrolusite structure has evolved and comprises a wealth of twin-boundaries rather than existing as a single crystal. (Twin) boundary regions are evidenced by observing where the parallel lines of Mn ions change direction.

In Figure 10, the Mn sublattice of six sequential Mn planes, cut perpendicular along [100], are shown to illustrate, more clearly, the wealth of twin boundaries. The figures are also annotated with oval/circle, square, and hexagon to highlight domains where the filling of the octahedra by Mn give rise to a zigzag configuration. It is perhaps disingenuous to describe these zigzag regions as reflecting a high density of twin boundaries. Accordingly, we suggest that these regions within the nanoparticle conform to the ramsdellite structure. In particular, the connectivities of the Mn ions are similar to those observed in Figure 8c, which are taken from experimental crystallographic coordinates for ramsdellite. However, although the configurations of these regions appear, by inspection, close to that of ramsdellite—they are certainly 1 × 2 Mn octahedra—there is considerable relaxation and rumpling of the ions comprising the nanoparticle, which arises from interfacial perturbation from the wealth of twin boundary regions, and surface relaxations. Interpretation of these structures as regions conforming to ramsdellite intergrowths must therefore be treated with caution. Nevertheless, we note further evidence for the ramsdellite structure can be drawn from the RDF data in Figure 6.

Inspection of the nanoparticle, using graphical techniques, reveals many Mn⁴⁺ vacancies that have evolved within the structure. Because the MnO₂ generated was stoichiometric, every Mn⁴⁺ vacancy must be charge compensated by either a Mn⁴⁺ interstitial or two O²⁻ vacancies − and both are observed. In
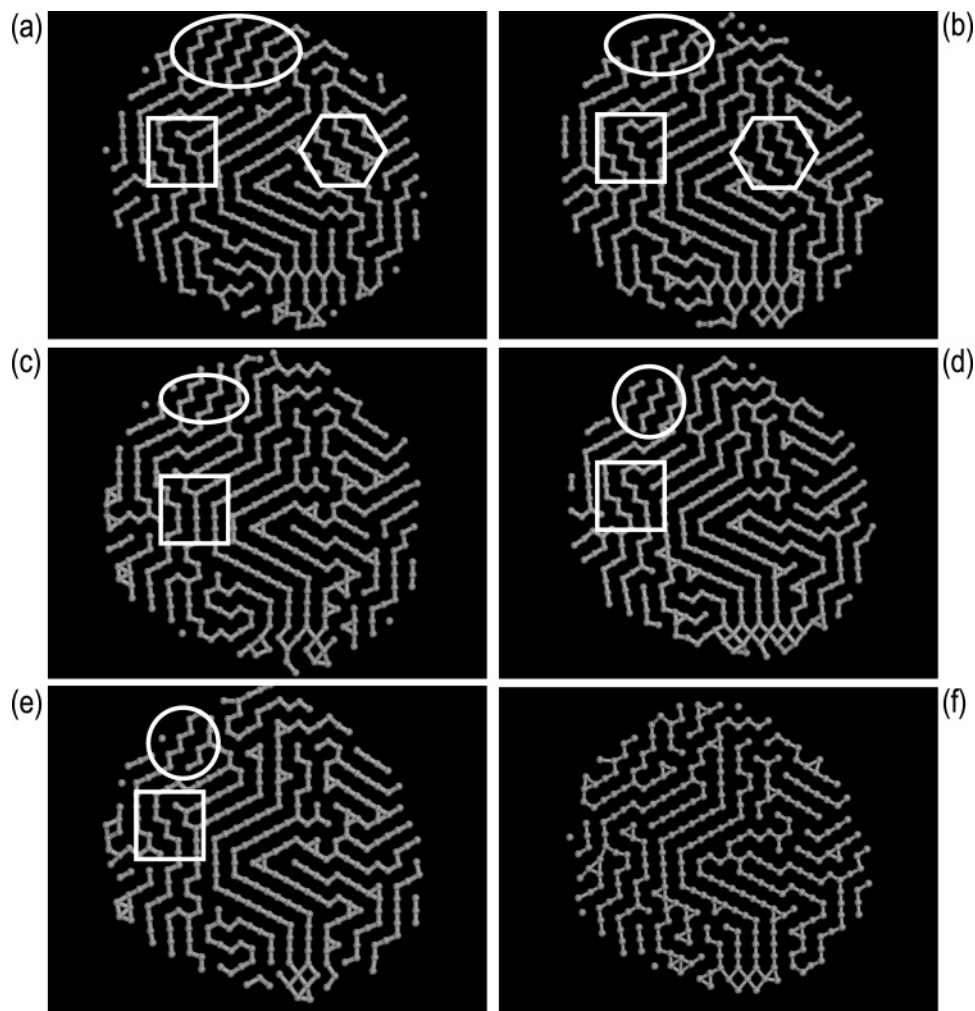
Figure 10. Slices cut sequentially through the nanoparticle, perpendicular to [100], depicting the Mn sublattice to help aid visualization of the 3D domains. Regions enclosed by circle/oval, square and hexagon are domains that we suggest may be interpreted as ramsdellite intergrowths (de-Wolff disorder).

addition to isolated Mn^{4+} vacancies, clusters, comprising multiple Mn^{4+} vacancies, are also present. These complex clusters also include oxygen vacancies, which we suggest are strongly bound to the Mn^{4+} vacancies because of the local charge imbalance created when a Mn^{4+} vacancy is formed. The structure of an isolated Mn^{4+} vacancy is shown in Figure 11 for illustration.

Discussion

An extensive study by Balachandran and co-workers,[26] who explored the structure of MnO_2 using density functional theory (DFT), showed that pyrolusite is the energetically favorable polymorph of MnO_2 in accord with our simulations. This confirms that our potential model can accurately describe the structure and properties of MnO_2 and inspires confidence in its application to explore the complex microstructural features associated with MnO_2.

EXAFS data on nanoparticles of MnO_2, about 10 nm in size (our model of the MnO_2 nanoparticle is 8 nm in diameter), revealed nearest neighbor Mn−O and Mn−Mn interatomic distances of 1.91, and 2.90 Å respectively,[19] which are very

close to our calculated values of 1.88 (Figure 6a) and 2.88 Å respectively. The experimental studies therefore help validate our models. The EXAFS data also suggests that the nanoparticles had "considerable absence of order in the long-range region." Our models for the MnO_2 nanoparticle are crystalline. However, our models accommodate very complex microstructures and the associated atomistic relaxation and rumpling are considerable. We suggest that the complex microstructure observed within our model together with the ionic relaxation and rumpling might help explain the absence of long-range order associated with the experimentally fabricated nanoparticles.

One can also estimate the crystallization speed from our simulation: In particular, the diameter of the nanoparticle is 8 nm and this takes about 1500 ps to crystallize (Figure 2a). Therefore, the crystallization front, at 2000 K, can be estimated to move at 8 nm/1500 ps or about 5 m/s.[27]

Conclusions

It is the microstructure of a material that governs its properties. However, generating a model that includes all the microstructural features, observed experimentally, within a

(26) Balachandran, D.; Morgan, D.; Ceder, G.; van der Walle, A. *J. Solid State Chem.* **2003**, *173*, 462.

(27) Albenze, E. J.; Thompson, M. O.; Clancy, P. *Phys. Rev. B* **2004**, *70*, art. No. 094110.
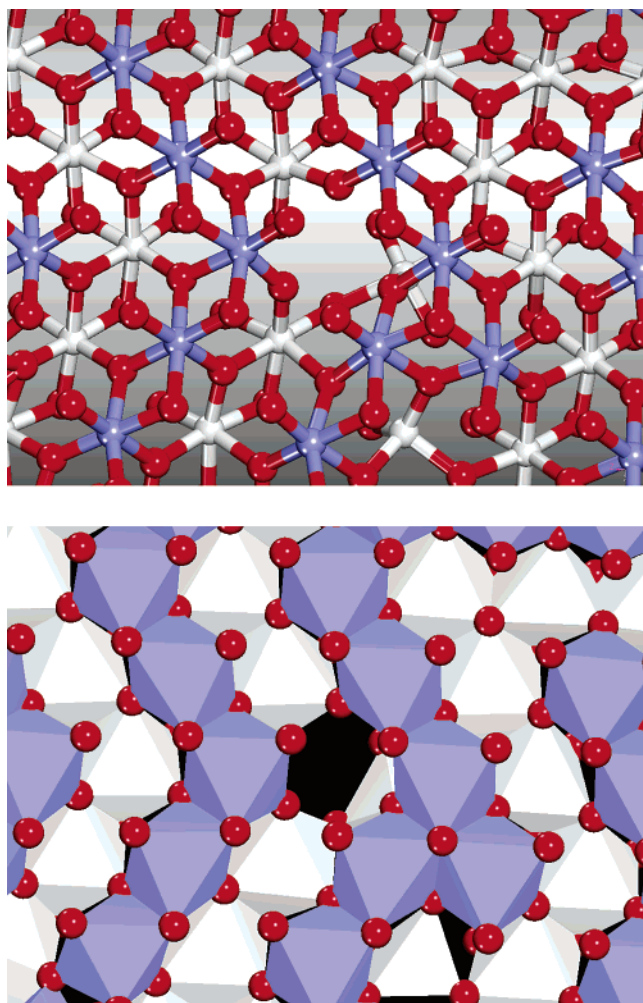
Figure 11. Segment cut through the nanoparticle showing the location of a Mn^{4+} vacancy (located at the center of each image) that has evolved within the MnO_2 lattice. (Top) Ball-and-stick representation of the atom positions. (Bottom) Polyhedral rendering of the octahedral sites occupied by the Mn^{4+} ions. Mn are colored blue (top layer) and white (bottom layer), and oxygen is red.

single simulation cell is very difficult to achieve. Fabrication of a material experimentally involves inevitably some kind of crystallization process. Indeed, it is the crystallization process that influences the microstructure and hence the properties of the material. Moreover, by controlling the crystallization process (whether recrystallization from solution, vapor deposition, molecular beam epitaxy, ball milling, etc.) one can exact some control over the microstructure and hence the properties of the material. Clearly, the ideal way of capturing, within a single model, the microstructural features observed experimentally, is to simulate the crystallization process itself. This is what we have endeavored to do in this study with the use of an amorphization and recrystallization strategy.

It is tempting to think, especially when viewing Figure 3, that one is observing "real" crystallization at the atomistic level. However, one must exercise caution in that the simulation is bound by simulation constraints implicit in the methodology—not least by the potential models describing the interactions between the ions. Conversely, it is very surprising that such highly complex microstructural features, observed experimentally, such as the wealth of twin-boundaries and isolated and associated point defects, have simply evolved in a purely artificial way within our simulations. Accordingly, we suggest that the simulated crystallization process we have shown in this present study must, at least in part, reflect crystallization that occurs in nature. Moreover, the models generated in this study can help experiment understand, with full atomistic detail, the considerable structural complexity of materials such as γ-MnO_2.

Supporting Information Available: Tables of calculated and experimental lattice parameters and structural parameters (PDF) and table of data in text format. This material is available free of charge via the Internet at http://pubs.acs.org.

JA0434073